THE JOURNAL OF PHYSICAL CHEMISTRY B

Article

Cite This: J. Phys. Chem. B 2018, 122, 10783−10792

pubs.acs.org/JPCB

Molecular Dynamics Simulations of Ion Selectivity in a Claudin-15 Paracellular Channel

Giulio Alberini,[†,‡] Fabio Benfenati,*[,†,§] and Luca Maragliano*[,†,§]

[†]Center for Synaptic Neuroscience and Technology (NSYN@UniGe), Istituto Italiano di Tecnologia, Largo Rosanna Benzi, 10, 16132 Genova, Italy

[‡]Department of Experimental Medicine, Università degli Studi di Genova, Viale Benedetto XV, 3, 16132 Genova, Italy

[§]IRCCS Ospedale Policlinico San Martino, Largo Rosanna Benzi, 10, 16132 Genova, Italy

Supporting Information

ABSTRACT: Claudins are tissue-specific transmembrane proteins able to form junctions between two cells and regulate the flow of physiological solutes parallel to the cell walls, that is, the paracellular transport. Claudin-15 is highly expressed in the intestine where it forms efficient Na^+ channels and Cl^- barriers. However, the molecular details of these biological complexes are still unclear. Here, the permeation process of Na^+, K^+, and Cl^- ions inside a refined structural model of a claudin-15 paracellular channel is investigated using all-atom molecular dynamics simulations in a double-bilayer and explicit solvent. One-dimensional potential of mean force (PMF) profiles, calculated using umbrella sampling (US) simulations, show that the channel allows the passage of the two physiological cations while excluding chloride. These features are generated by the action of several acidic residues, in particular the ring of D55 residues which is located at the narrowest region of the pore, in correspondence with the energy minimum for cations and the peak for chloride. We also used the Voronoi-tessellated milestoning method to obtain additional PMF profiles and the permeation timescale of the three ions. The milestoning PMFs agree well with those obtained by US, and the rate calculation reveals that the passage of chloride is almost 30 times slower than that of sodium. Our results are consistent with the known ability of claudin-15 to regulate tight junction selectivity and with the experimentally determined role of the acidic residues. This further validates our structural model and provides insights into the atomistic details of ion transport in paracellular channels that could be shared by other claudin-based architectures.

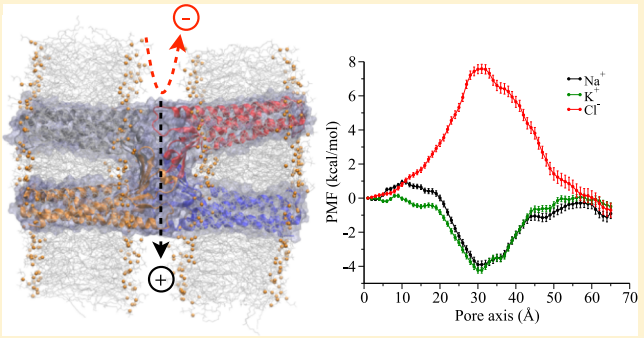

INTRODUCTION

The blood−brain, renal, and intestinal barriers are examples of highly selective biological barriers that separate distinct compartments and maintain stable chemical−physical conditions. They are formed by tightly bound epithelial or endothelial cells, whose lateral membranes are connected via regions of narrow space named tight junctions (TJs) composed of several proteins organized in strands.[1−6] TJ proteins are responsible for regulating the paracellular transport of solutes via charge- and size-selectivity mechanisms,[7,8] and their malfunction is associated with numerous diseases. Because of this, understanding their molecular mechanisms and dysfunctions has a very high clinical potential.[9]

Two main families of membrane proteins constitute the TJ strands, namely the occludins and the claudins. In particular, claudins alone recapitulate the TJ structural/functional features with tissue-specific expression[10] and appear as strands under freeze-fracture electron microscopy (EM).[11] To form TJs, the claudins assemble via cis (intracellular) interactions along the individual cell membrane and via trans (intercellular) interactions, across adjacent cells.

A preliminary classification divides the claudin proteins on the basis of their action as barriers or pores for small solutes.[12] Although only a few claudins unequivocally qualify as pore-forming claudins, an extensive literature suggests that the paracellular space is never completely occluded, also for barrier-like claudins.[13−16] Functional studies of paracellular permeability have shown that there are at least two types of pore channels: a high-capacity pathway with an estimated pore radius of about 4 Å and a low-capacity pathway with a pore radius of at least 7 Å.[17] Claudin proteins fold into a four-transmembrane helix bundle (TM1−4) with two extracellular loops (ECL1−2), cytoplasmic terminal residues, and an intracellular loop.[18] Biochemical investigations have helped identifying the residues important for cis and trans interactions, as well as the pore-lining residues. Furthermore, the crystal structure of mouse claudin-15 (mCldn15) was resolved[18] (PDB ID: 4P79). Two other crystal structures of claudins were

Received: July 6, 2018
Revised: October 29, 2018
Published: October 29, 2018

DOI: 10.1021/acs.jpcb.8b06484
J. Phys. Chem. B 2018, 122, 10783−10792

obtained afterward (mCldn19[19] and hCldn4[20]) in complex with the *Clostridium perfringens* enterotoxin, elucidating the molecular basis of TJ disruption. However, these structures are not sufficient to univocally describe the functional TJ architecture.

Highly expressed in the intestine, Cldn15 belongs, together with Cldn2, to a family of claudins characterized by a high TJ permeability to cations.[21] Specifically, Cldn15 protomers form selective pores that are channels for Na^+ and highly resistant barriers to Cl^- ions. The crystal structure of Cldn15 has opened a new phase in the molecular study of paracellular transport. Indeed, the monomeric structure of Cldn15 has been studied with coarse-grained (CG) simulations[22] and used as a template to build structural models of other claudins.[23−25]

Furthermore, soon after the publication of the Cldn15 crystal, a model of paracellular channels (from now on referred to as the Suzuki model) was proposed using the same structure.[26] A detailed description of this model can be found in the Supporting Information. The putative architecture predicts the formation of β-barrel like channels with a diameter smaller than 10 Å through the association of antiparallel double rows of claudins in adjacent membranes. Such an arrangement is supported by cysteine cross-linking data, and it is consistent with freeze-fracture EM images of polymeric TJ strands. Moreover, it displays negatively charged pore-facing (D55) and pore-lining (D64) residues, whose mutation was shown to reverse the pore selectivity for cations.[27] As a further support for the Suzuki model, computational studies based on CG models[23−25] showed that various claudin homologs of Cldn15 spontaneously associate in similar pore structures. Nevertheless, the validity of the Suzuki model as a general template for TJ pores is still debated.[28]

In our previous work,[29] we used all-atom molecular dynamics (MD) simulations to obtain refined models of single- and double-paracellular pores formed by trans-interacting Cldn15 dimers and tetramers, assembled as in the Suzuki model and embedded in double-bilayer and water environments. The structures preserve the main features of the original model, showing stable cis and trans interactions between monomers, and a stationary minimum pore diameter of 5−6 Å. More recently, a double-pore structure, similar to our prediction, was shown to be stable in MD simulations over longer timescales.[30]

Moreover, two very recent studies explored selectivity in paracellular channels using atomistic simulations. In ref 25, a simulation of a Cldn2 pore, similar to the Suzuki model, was performed. Along the simulated trajectory, the authors observed the permeation of 13 Na^+ and only 1 Cl^-, consistent with the cation selectivity properties of Cldn2. More recently, in ref 31, an MD-refined version of the Suzuki model for Cldn15 was also proposed, and its selectivity was confirmed by measuring the ionic currents.

Here, we further validate our single-pore model by investigating its selectivity properties for cations using atomistic MD simulations. To this aim, we employ the umbrella sampling (US)[32] method for free energy (FE, or potential of mean force, PMF) and the Voronoi-tessellated milestoning[33,34] method for PMF and kinetics calculations to study the permeation of ions through the channel. Our simulations confirm the cation selectivity nature of the Cldn15 channel structure and provide a quantitative explanation of the mechanism as governed by an attractive energy minimum at the binding site for cations and a repulsive barrier for anions. Moreover, they provide valuable atom-level detail on the ion permeation process, confirming the role of acidic residues inferred from experiments,[27] particularly D55.

COMPUTATIONAL METHODS

US Simulations. In US calculations,[32] a harmonic potential energy term is added to the MD potential to ensure efficient sampling along the chosen collective variable (CV) in different independent simulations (named *windows*). In the case of one-dimensional (1D) CV used here, indicated as z, these potentials are expressed as

$$\hat{\omega}_i(z) = \frac{1}{2}\hat{\kappa}(z - z_i^0)^2 \tag{1}$$

where z_i^0 indicates the value at which the CV is restrained in window i and $\hat{\kappa}$ is a constant. For an appropriate choice of $\hat{\kappa}$, a sufficient overlap between the sampled distributions of adjacent windows is obtained, and the full PMF profile can be reconstructed with the weighted histogram analysis method (WHAM).[35,36]

Milestoning MD Simulations. The reaction rate estimations based on PMF profiles require assumptions that are often hard to satisfy in biomolecular systems, such as a dominant transition state or no recrossings at the barrier. Alternatively, several enhanced sampling techniques have been developed over the years to calculate the rates from MD simulations.[33,37−39] milestoning[33] allows reconstructing the long-time dynamics of a system by exploiting its crossing statistics through a set of hypersurfaces placed along the reaction coordinate. Voronoi-tessellated Markovian milestoning[40,41] is a version of the method that relies on independent simulations confined within a set of cells spanning the reaction coordinate and uses transition path theory[42] to obtain the kinetic properties of the full reaction from hitting statistics at the cell boundaries.

In Voronoi-tessellated milestoning,[40] several MD simulations are confined within cells that span the space between metastable states, and the kinetic properties of the transition are reconstructed from the hittings on the cell boundaries, identified as milestones. If we consider a set of M points in the CV z-space (z_1, z_2, ..., z_M), usually called centers, these partition the configuration space in M Voronoi cells. The Voronoi cell associated to z_α is identified as the region of space where each point is closer to z_α than to any other center z_β. It was shown in ref 40 that the statistical properties of the longtime dynamics of a system can be reconstructed from independent simulations, properly confined within each of the Voronoi cells. More specifically, the confinement must leave unperturbed the dynamical properties of the systems when it is in the interior of the cell as well as the probability flux in and out of the cells. Such a confinement was realized in ref 40 by using velocity reflections at the cell boundaries.

Soft-Walls Restraining Potentials. An alternative strategy to confine the CV in the Voronoi cells was proposed in ref 34 and amounts to use half-pseudoharmonic restraining potentials (termed *soft-walls*). This approach was demonstrated to yield the same results of the original one and to allow much easier interfacing with the highly optimized, widely used biomolecular simulation MD packages. It requires that the portions of trajectories that are transiently out of the cells are discarded in the analysis, but this effect is minimized by proper tuning of the parameters.

DOI: 10.1021/acs.jpcb.8b06484
J. Phys. Chem. B 2018, 122, 10783−10792

In the case of 1D CV used here, z, the soft-walls potentials acting in each of the Voronoi cells defined by the z_α points are expressed as

$$\tilde{\omega}_\alpha(z) = \begin{cases} \frac{1}{2}\tilde{\kappa}(z - z^\alpha_{\text{upper}})^2 & \text{if } z > z^\alpha_{\text{upper}} \\ 0 & \text{if } z^\alpha_{\text{lower}} \le z \le z^\alpha_{\text{upper}}, \text{ centered in } z_\alpha \\ \frac{1}{2}\tilde{\kappa}(z - z^\alpha_{\text{lower}})^2 & \text{if } z < z^\alpha_{\text{lower}} \end{cases} \quad (2)$$

where z^α_{lower} and z^α_{upper} denote the edges of the cell and are the midpoints between the center z_α and the adjacent ones.

Rate Calculation. By considering the edges of the Voronoi cells as milestones, the dynamics of the system can be reduced to that of a discrete-state continuous-time Markov chain in the state space of milestone indices. This amounts to define a rate matrix q_{ij}, with i and j indexes of milestones, whose elements are given by $q_{ij} = N_{ij}/R_i$, where N_{ij} is the number of transitions from i to j, and R_i is the total time that milestone i was the last crossed. These factors can be expressed in terms of quantities extracted from the confined simulations, that is, if we indicate with α the cell index: $N_{ij} = \sum_{\alpha=1}^{M} \pi_\alpha (N_{ij}^\alpha / T_\alpha)$ and $R_i = \sum_{\alpha=1}^{M} \pi_\alpha (R_i^\alpha / T_\alpha)$. Here, π_α is the equilibrium probability of finding the system in cell α, T_α is the duration of the simulation in the cell, and N_{ij}^α and R_i^α are defined as N_{ij} and R_i, but for the simulation in α. The PMF associated to the cells is obtained as $-k_B T \ln(\pi_\alpha)$,[40] whereas the mean first passage times (MFPTs, inverse of the rates) from any milestone to any other are calculated from the matrix q_{ij} by solving a linear system, as reported in refs.[34,40] In our study, we compute the MFPT from a milestone located at the mouth of the channel to a milestone located at the opposite mouth. As we are interested in the relative permeation timescales of the ions, and because there are only one entry and one exit portal in our structure, we neglect the entry kinetics contributions related to bulk concentration and diffusivity that are discussed in ref 41.

Protocols of the System Setup. *Configuration of the Cldn15 Channel and MD Parameters.* An equilibrated configuration of the single-pore model described in our previous work[29] was extracted and used as the starting conformation in all enhanced MD simulations described here (see Figure 1). Briefly, the model includes four Cldn15 protomers (two for each cis configuration), two membrane bilayers formed by 1-palmitoyl-2-oleoyl-*sn*-glycero-3-phosphocholine (POPC) molecules (~280 for each bilayer), water molecules, and four sodium ions, for a total of 164 814 atoms. All the simulations were performed with an *NPT* ensemble (P = 1 bar, T = 310 K), maintained by a Nosé–Hoover Langevin piston pressure control and a Langevin thermostat.[43,44] The NAMD 2.12 software was used[45] with the CHARMM36 force field[46,47] for proteins and lipids, performing Langevin dynamics. The water molecules were described with the three-point TIP3P model[48] and the ions with the parameters included in the force field. The environment is assumed at a neutral pH = 7, and the acidic amino acids have deprotonated side chains. Electrostatic and van der Waals interactions were calculated with a cutoff of 12 Å and the application of a smoothing decay starting to take effect at 10 Å. Hexagonal periodic boundary conditions implemented in NAMD were used and long-range electrostatic interactions were calculated using the particle mesh Ewald algorithm.[49] All covalent bonds involving hydrogen atoms were kept fixed using SHAKE[50]/SETTLE algorithms to allow the use of a timestep of 2 fs. To ensure maximum accuracy, the electrostatic and van der Waals interactions were computed at each simulation step.

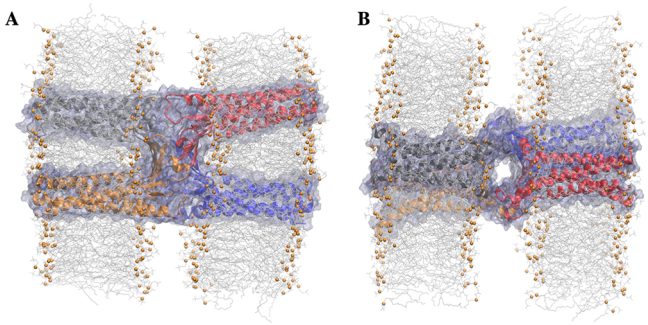

Figure 1. Representations of the equilibrated single-pore configuration used in all MD calculations: the equilibrated configuration of the Cldn15 paracellular channel extracted from the MD trajectory described in ref 29. The system is viewed from the lateral (A) and the apical (B) side. The four Cldn15 protomers are shown in cartoon style with different colors (red, dark blue, dark gray, and orange). The whole protein complex is also reported as a blue surface to visualize the walls of the channel in panel A and the pore region in panel B. Membrane POPC lipids are shown as gray lines and the phosphorus atoms as orange spheres. Solvent molecules in the three compartments are not shown for clarity.

One-dimensional US simulations with harmonic biases were performed with the CV interfaces (Colvars library),[51] using as single CV the projection of the ion position onto the axis of the paracellular channel. The WHAM code from the Grossfield group, available at http://membrane.urmc.rochester.edu/content/wham, was used to reconstruct the 1D PMF. This is a natural choice in ion permeation studies, and the convergence of our results confirmed it as appropriate for this channel also. The Colvar plugin was also used to apply the half-harmonic restraints of milestoning MD simulations with the same CV of the US simulations. As we used absolute cartesian coordinates of the ions as CVs, to avoid any rigid body rotational or translational displacement of the channel, we applied harmonic restraints to the Cα atoms of the residues 11, 20, 80, 94, 122, 133, 167, and 177 (all in the transmembrane domains of the proteins). To optimize the use of parallel computational resources, for all the US and milestoning MD simulations, we prepared a number of starting conformations, where the tested ion was swapped with equilibrated water molecules, for the whole length of the paracellular channel. For each configuration, the test ion was kept fixed, together with the proteins and the lipids, during 1000 steps of energy minimization and more than 1 ns of MD to allow the equilibration of water molecules. We verified that in all the US and milestoning simulations, the channel architecture maintains its integrity and the ion never leaves the pore via a direction perpendicular to its axis. All trajectories were visualized and analyzed using UCSF Chimera[52] and VMD with their associated plugins.[53]

Details of US Calculations. We performed US simulations with the harmonic restraints of eq 1, and $\hat{\kappa}$ = 2 kcal/(mol·Å^2). We employed a total of 65 umbrella windows with a uniform spacing of 1 Å. In each window, the simulation lasted 5 ns, and the first 500 ps were not used in the analysis. For WHAM analysis, we used 600 bins and a tolerance of 0.0001. Errors were calculated via bootstrapping using 100 trials for each PMF. As bootstrap analyses might underestimate the errors in

DOI: 10.1021/acs.jpcb.8b06484
J. Phys. Chem. B 2018, 122, 10783–10792

US simulations, we also computed the error estimates by block analysis (see the Supporting Information). We divided the trajectory in each window in four consecutive blocks and calculated the PMF profile as an average of those obtained with WHAM in each of the last three, with the errors computed as standard deviations. Overall, the US calculations are based on a cumulative production of ∼975 ns.

Details of Milestoning Calculations. Voronoi-tessellated Milestoning MD simulations were performed to evaluate the PMF and the kinetic properties of the Na^+, K^+, and Cl^- ions. For each ion, the length of the channel was mapped using 23 cells. Pseudoharmonic restraining potentials, with $\tilde{\kappa}$ = 100 kcal/(mol·Å^2) in eq 2, were applied to restrain the permeating ion in each cell. The simulations lasted for 3 ns per cell for sodium and potassium and 6 ns per cell for chloride. The first 100 ps of each trajectory were not considered in the data analysis. Overall, these calculations are based on a cumulative production of ∼276 ns. All MD simulations performed for PMF and MFPT calculations are summarized in Table 1.

Table 1. Summary of the MD Simulations Conducted for PMF and Kinetic Calculations

simulation type	molecule	cumulative simulation length (ns)
US	Na^+	325
US	K^+	325
US	Cl^-	325
milestoning	Na^+	∼69
milestoning	K^+	∼69
milestoning	Cl^-	∼138

Additional Unbiased MD Simulations. Finally, we extended the main simulation of the single-pore channel reported in ref 29, adding ∼140 ns (reaching a total of about ∼400 ns) to monitor the structural stability and pore dimensions of the system. The MD setup is the same as that of the original paper. The HOLE software[54,55] was used for the calculations of the pore dimensions.

RESULTS

This section is organized in two paragraphs. In the first one, we describe the results of 1D US and Voronoi-tessellated milestoning calculations for Na^+, K^+, and Cl^- ions. In the second paragraph, we report on the structural features of the pore analyzed after extending the simulation described in ref 29 and the observed Na^+ hydration at the binding site.

PMF Calculations and Ion Permeation Rates. A wealth of experimental data confirms that Cldn15 paracellular channels are highly selective for cations, particularly Na^+. To verify the effect of channel structure and amino acid composition on ion permeation, we used the US and Voronoi-tessellated milestoning methods to perform PMF and kinetics calculations for Na^+, K^+, and Cl^-, using in all cases the position of the ion along the pore axis as CV (Figure 2).

The US PMF profiles are reported in Figure 3, with the errors estimated via bootstrapping (errors from the block analysis described in the Computational Methods section can be found in Figure S4). All curves show one main feature and are symmetric with respect to the center of the channel. The profiles of Na^+ and K^+ reveal a minimum, in both cases about 4 kcal/mol deep, whereas that of Cl^- shows a large barrier of about 8 kcal/mol. Remarkably, the shape of the profiles correlates with the position of the acidic residues and the

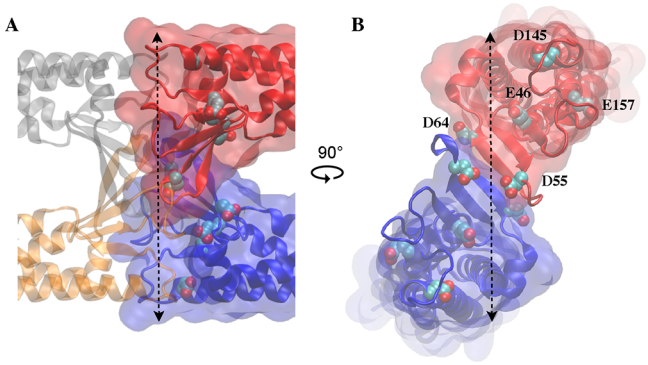

Figure 2. Amino acid composition of the paracellular pore surface: (A) lateral, zoomed view of the Cldn15 TJ pore, with the protomers depicted as in Figure 1, and surface representation used for protomers 1 and 2 only; the side chains of acidic residues in protomers 1 and 2 are shown as spheres; the dashed line represents the axis used in the simulations of ion permeation. (B) Cut-away view of the channel, showing only protomers 1 and 2 for clarity, with the acidic residue numbering indicated for protomer 1. Note that the β-strands are tilted with respect to the channel axis, as in β-barrel structures.

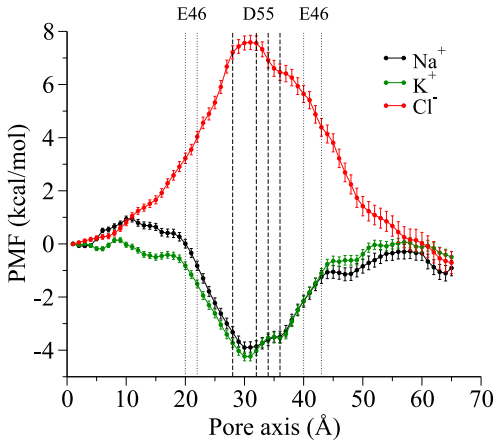

Figure 3. Energetics of ion permeation: PMF profiles for the permeation of sodium (black), potassium (green), and chloride (red), obtained from US−WHAM calculations. The error estimation for each window, obtained with bootstrap analysis, is represented with bars. The position of the C_α atoms of D55 and E46 residues are represented as dashed and dotted lines, respectively.

narrowing of the channel toward its center. Indeed, by observing the channel structure, several negatively charged residues might drive the flux of Na^+ ions through the pore and hinder that of Cl^-. Moving from the mouth of the channel toward the narrow center, these residues are, in each protomer (see Figure 2), D145 (whose side chains point toward the channel interior), E157 (side chains toward the exterior), E46 (internal side chains), D64 (external side chains), and D55 (internal side chains). Conversely, there are only two basic amino acids per protomer in the paracellular space, R30 and K155, both located at the mouth of the channel, where the pore is wider. The side chain of K155 points toward the exterior of the channel, whereas that of R30 points toward a transmembrane helix, and it is tangential to the channel walls. The positions of all these residues are symmetrical to the channel axis and the channel center. With respect to the PMF profiles in Figure 3, the Cα atoms of D64 are at the level of windows at 25 and 38 Å and those of E46 at 20, 22, 40, and 43

DOI: 10.1021/acs.jpcb.8b06484
J. Phys. Chem. B 2018, 122, 10783−10792

Å. The positions of D55, corresponding to the narrow region of the pore, are at 28, 32, 34, and 36 Å and coincide with the minimum in the cation PMF and the maximum in the anion PMF.

The PMF profiles from Voronoi-tessellated milestoning are shown in Figure 4. The curves agree well with those from US,

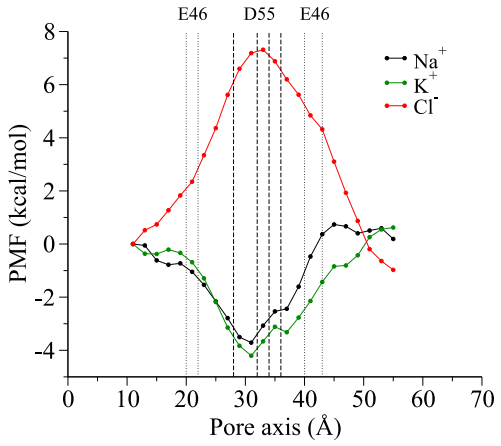

Figure 4. Energetics of ion permeation: PMF profiles for the permeation of sodium (black), potassium (green), and chloride (red), obtained from milestoning MD simulations.

showing a single minimum of about 4 kcal/mol deep for the cations and a single barrier of almost 8 kcal/mol for chloride, again in correspondence with the D55 residues. The MFPTs of ion permeation through the channel (cumulative from the first milestone to all the successive ones) are shown in Figure 5 as a

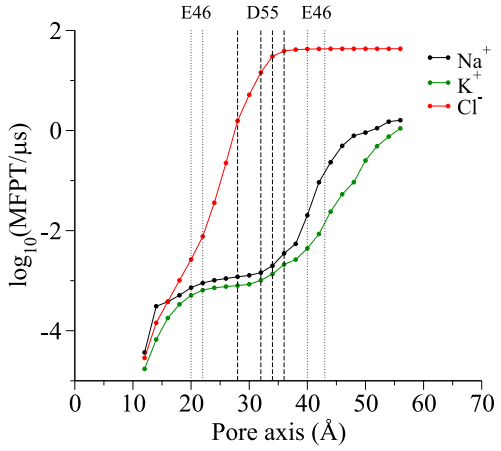

Figure 5. Kinetics of ion permeation: MFPTs along the pore axis from milestoning MD simulations.

function of the coordinate along the channel axis. As can be observed, the timescales of cation permeation are quite similar, with the transition occurring on the microsecond scale, whereas that of Cl^- is longer, further confirming the high channel selectivity for cations. Specific values of the total MFPTs for the transitions are reported in Table 2.

Pore Size and Hydration of Na^+ during Permeation. To further assess the structural stability of our model, and investigate over a longer timescale the dynamics of the pore size and how this affects ion permeation, we have extended the unbiased 250 ns MD trajectory presented in ref 29, reaching ~400 ns. The root-mean-square deviations (RMSDs) of the

Table 2. MFPTs and Relative Rates of Single Ion Permeation through the Cldn15 Paracellular Channel

ion	MFPT (μs)	relative rate
Na^+	1.6	1
K^+	1.1	1.4
Cl^-	43.1	0.04

backbone atoms of each protomer, shown in Figure 6A, are stationary around plateaus at 2 Å, revealing a stable global

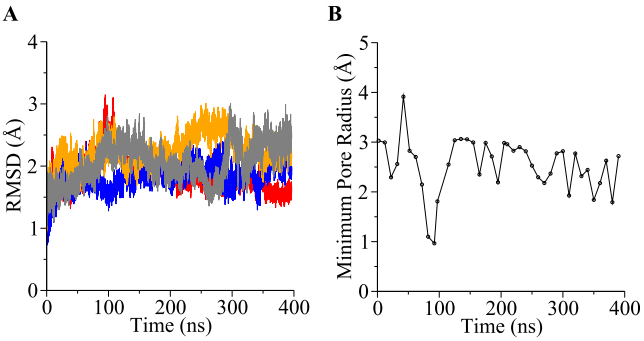

Figure 6. Structural features of the system in the unbiased MD simulations: (A) RMSD values of the backbone atoms of the four protomers along the entire MD trajectory and (B) minimal pore radius along the trajectory.

structure over the entire analyzed trajectory. Interestingly, the minimum pore size remains stationary around 5−6 Å (Figure 6B), in agreement with the available experimental results for another pore-forming, cation-selective, claudin (Cldn2).[56] The pore size critically affects the hydration state of the ion during permeation. In the Cldn15 channel, the D55 ring is located at the narrow region of the pore, so that size and electrostatic effects combine to determine selectivity.

To investigate this mechanism, we analyzed the hydration state of the Na^+ ion over the permeation pathway from the US calculations. We computed the number of oxygen atoms from water molecules and protein residues coordinating the Na^+ ion in the first hydration shell (using 3.0 Å as the threshold). In Figure 7, we show the average number of water molecules

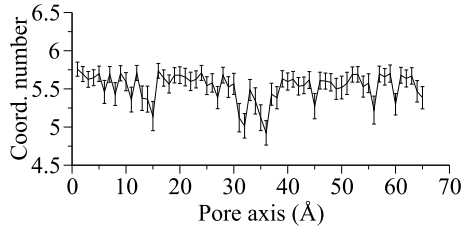

Figure 7. Average number of sodium-coordinating water molecules in US windows as a function of the reaction coordinate.

around the sodium ion in each US window, as a function of the reaction coordinate. Although limited dehydration events can be observed along the channel, the most pronounced ones occur at the middle of the pore, where the cage of four D55 residues is located (windows 28−36). To investigate more in detail this effect, in Figure 8, we show the results for the US windows at 2 and 32 Å, located near the mouth of the channel and at the central D55 ring site, respectively. In the most external window, the ion is fully solvated (the average number

DOI: 10.1021/acs.jpcb.8b06484
J. Phys. Chem. B 2018, 122, 10783−10792

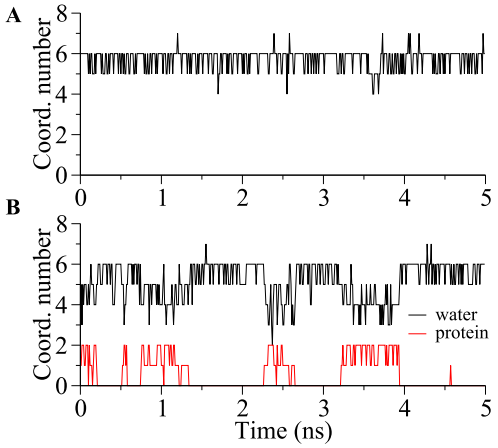

Figure 8. Number of oxygen atoms coordinating the Na^+ ion in US windows: (A) window at 2 Å and (B) window at 32 Å; the black line indicates the coordinating oxygen atoms from water molecules, whereas the red line indicates those from the D55 side chains.

of coordinating water molecules is 5.7 ± 0.1). Conversely, when in the narrow channel region, the Na^+ ion occasionally loses one or more hydrating water molecules, replaced by oxygens from the side chains of D55.

To confirm this observation, we also looked at the entire unbiased MD trajectory and indeed found a time window in which a Na^+ ion in the paracellular space spontaneously enters the channel and binds to aspartic acids of the ring in a partially dehydrated state. In Figure 9, we report two snapshots

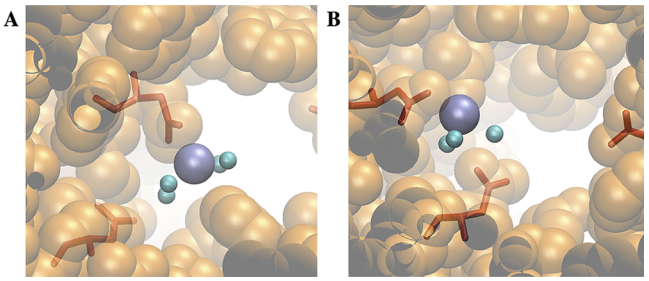

Figure 9. Partial dehydration events of a Na^+ ion in the central pore region: (A) snapshot extracted from the US simulation window at 32 Å and (B) snapshot extracted from the unbiased MD simulation. The ice-blue sphere is the Na^+ ion, small cyan spheres represent water molecules in the hydration shell of the ion, whereas all other water molecules in the system are not shown. The side chains of the D55 residues involved in ion binding are represented as red sticks, and the protein is represented as an orange vdW sphere.

representing such partial dehydration events. Globally, these findings are consistent with the mechanism hypothesized in ref 56 for the cation-selective Cldn2 channel, where a partial dehydration process is coupled to a pore diameter of 6.5 ± 0.3 Å. Indeed, such a pore size, as well as the one we obtain for Cldn15, closely corresponds to the diameter of a hydrated Na^+ ion (6−7 Å), so that Na^+ would likely have to shed at least a part of its hydration shell during permeation.

DISCUSSION

The concept of charge selectivity is widely used to illustrate the ability of channel proteins to regulate the flux of various ions via the action of charged residues at specific sites (for claudin's charge selectivity, see in particular ref 57). As atom-detail structures have become available, many computational studies investigated the selectivity properties of transmembrane ion channels such as potassium[58−61] and sodium[62−66] channels. On the contrary, because of the lack of structural information, the simulation studies of paracellular channels are only starting to appear.

Starting from the Suzuki model of the TJ paracellular channel of Cldn15, we recently generated a refined, all-atom structural model of a Cldn15 channel.[29] Being built from a crystal structure and based on experimental data, the Suzuki architecture seems to be the most appropriate initial structure for simulation studies of paracellular channels. Our model proved to be stable in MD simulations by preserving the residue−residue cis and trans interactions between monomers known from experiments to be critical for the TJ strand formation. Moreover, it showed a minimal pore size of 5−6 Å that remained stationary along the simulated trajectory.

Given that both the Cldn15 monomer crystal and the Suzuki model were published quite recently, only a few MD studies of paracellular channels have appeared so far. In a series of papers,[23−25] Nangia and collaborators used CG models to investigate the intramembrane association of dimers of distinct claudins (modeled by homology with Cldn15) and generated all-atom, single-pore models via head-to-head docking of these dimers. Their findings suggest pores consistent with the Suzuki model, and that the tissue-specific properties of paracellular channels from different claudins might originate from the differences in the amino acid sequence along the extracellular loops. In ref 25, the authors describe a Suzuki-like single pore of Cldn15, but do not perform MD simulations of it. They claim their model shows a diameter of 7 Å at the narrowest point, near the D55 ring. Our model, coming directly from the Suzuki one, shows an average minimal diameter of around 5−6 Å at the same location, stable over the 400 ns MD simulations.

In another study,[30] atomistic MD simulations showed a partial loss of structure in a Cldn15 strand of 16 protomers forming four pores, assembled based on the Suzuki model. However, the same work showed stable double-pore configurations, as we also found in our previous study.[29] Together with ours, these results point to the validity of the Suzuki model at least for single- or double-pore conformations. More recently, another all-atom MD-refined version of the Cldn15 Suzuki model has become available.[31] The authors rely on the periodic replicas of the simulation box to build a virtually continuous strand of channels from a unit cell of three and observe that stable pore architectures are maintained by the same cis and trans interactions between monomers we identified in ref 29. From their simulations, they obtain a mean diameter of 8.4 Å at the narrowest pore region, a bit larger than that in our model. Overall, it is remarkable that, regardless of the minor differences in the protocols followed to complete the missing protein segments and to assemble the intermembrane architecture, several independent studies demonstrated the plausibility of the paracellular channel putative structure of the Suzuki model.

In addition to the structural features, however, a reliable model has to recapitulate the physiological properties of the system it represents. Here, we further validated our single-pore structure by verifying that it correctly reproduces the experimentally known selectivity of Cldn15 pores for cations.[67,68] To this aim, we applied the US method to calculate the PMF for single-ion permeation through the channel, using Na^+, K^+, and Cl^- ions, and the Voronoi-

DOI: 10.1021/acs.jpcb.8b06484
J. Phys. Chem. B 2018, 122, 10783−10792

tessellated milestoning technique to determine again the PMF and kinetic rates for the same process. In all cases, we used the position of the ion along the main axis of the channel as CV.

The PMF curves obtained from US and milestoning are symmetrical with respect to the channel center, consistent with the symmetric structure of the tetrameric pore. From a functional point of view, symmetric conductance was observed in Cldn2 cation channels, indicating ion fluxes electrochemically driven by a concentration gradient between the opposite ends.[69] The PMF profiles show a single minimum of about 4 kcal/mol deep for Na^+ and K^+ and a barrier of about 8 kcal/mol for Cl^-, centered at the narrowest region of the channel. These features well correlate with the distribution of amino acids along the pore. Indeed, the structure displays several negatively charged residues from the different protomers lining the pore surface in symmetrical positions with respect to the main axis, capable of generating an electric potential to drive the flux of cations and hinder that of anions. Among these acidic residues, the four D55 residues are located at the center of the pore, where the PMF profiles show the minima and the peak of the barrier. These results show that our structural model of the Cldn15 channel preserves the required selectivity for cations and substantiate the experimental observation that selectivity is mostly regulated by the D55 residues.[21,31]

The permeation timescales for the Na^+, K^+, and Cl^- ions, calculated using soft-walls Voronoi-based milestoning in 1D, yielded ratios of permeation rates that again confirm that our Cldn15 channel model replicates the marked charge discrimination of cation-selective paracellular channels. It is important to stress that we performed calculations for single-ion permeation only, whereas the actual transport properties might result from the crossing of multiple ions. However, the single-ion PMF is a central concept in the models of permeation, determining conduction at a relatively low ion concentration[70] and providing fundamental features of the process as, for example, the location of binding sites and repulsive barriers, or the relative magnitude of the protein interaction with distinct ions. It is also important to remark that, although multiple experiments unequivocally identify Cldn15-containing TJs as strongly cation-selective[21,31] and attribute to Cldn15 the major contribution, an absolute estimate of selectivity for these proteins is lacking. This is due to the concurrent role of other cation-selective claudins in the same junctions (e.g., Cldn2) and because measures are made as variations of selectivity from normal cells after knocking down or overexpressing Cldn15 or its mutants.[21] This notwithstanding, by yielding a ratio of 0.04 between the anion and cation rates, our calculations are consistent with the available experimental observations in revealing a high selectivity of Cldn15 channels for positive ions.

Two other studies investigated paracellular selectivity using atomistic simulations, and they are both extremely recent. In ref 25, the authors performed a 300 ns long all-atom MD simulations of a Cldn2 pore (also cation-selective) similar to the Suzuki model, but obtained from docking, and observed permeation of 13 Na^+ and only 1 Cl^-. These simulations provide a valuable, albeit qualitative, description of selectivity. Moreover, although Cldn2 shares an overall high degree of sequence similarity with Cldn15, substantial differences in the amino acid compositions, particularly at the pore-forming β-strands, could lead to different scenarios for sodium transport in the two systems.

Even more recently, Samanta et al.,[31] using all-atom MD simulations, investigated the selectivity of the transport properties of a Cldn15 paracellular pores model by calculating ionic currents from the simulated trajectories of sodium, other small positively charged molecules, and chloride under the application of a constant external electric field. Our results about cation selectivity and the role of D55 residue well agree with those in ref 31. In addition, we provide a quantitative link between the ion permeation mechanism and the structure of the channel, in terms of an attractive energy well at the cation-binding site and a repulsive energy barrier for the anion.

In all-atom MD simulations, both ionic current calculations under external electric fields and enhanced PMF calculations are widely used to investigate the conduction and selectivity mechanisms of transmembrane channels. Remarkable examples include studies of potassium[59,71,72] and, more recently, sodium[62,63,65] channels. Although the current provides a direct measure of conduction, it requires a statistically sufficient sampling of ion-crossing events, which implies long simulated trajectories or high applied voltages that can affect the channel structure and/or its mechanism. Ion fluxes, however, are ultimately determined by the energetically favorable/unfavorable sites encountered by the particles inside the protein, and a detailed map of these features is provided by PMF calculations. Hence, PMF maps and profiles allow a quantitative interpretation of the experimentally determined conduction in terms of the protein's amino acid composition and conformation.[70,73] In addition, for the specific case of paracellular channels considered here, ionic current calculations require sealing the paracellular space with multiple pores to avoid the passage of ions in the aqueous environment between bilayers, thus considerably increasing the size of the simulated system. The PMF and rate calculations, conversely, while permitting the use of a smaller, single-pore structure, also yield the thermodynamic and kinetic properties of the individual conducting unit that are required to interpret the TJ electrophysiology experiments using single-channel models.[56,69]

The observation that the minimal pore size of our Cldn15 channel is stationary around 5−6 Å, close to the size of a hydrated Na^+ atom, pushed us to investigate the details of ion hydration during permeation. Indeed, electrostatic and steric effects couple to determine ion transport in most channels, and pore width-related ion dehydration effects are known to be relevant in narrow channels such as gramicidin[74] or in the selectivity filter of potassium[60,61] and sodium[62] channels. By inspection of the restrained simulations for PMF calculations and of the unrestrained MD trajectory, we observed that, when in close proximity to the acidic amino acids, the Na^+ ion can shed one or two water molecules from its hydration shell by substituting them with oxygens from the side chains of the residues. A similar mechanism was hypothesized to characterize Na^+ permeation through Cldn2 channels in ref 56, after the experimental estimates of pore size and permeability. However, as we obtain very similar PMF profiles for sodium and potassium, our results suggest that electrostatic interactions, and not hydration patterns, play a major role in selectivity, at least for Cldn15.

Our calculations of PMF and timescales of ion permeation through the Cldn15 pore reveal interesting details on the mechanism of ion transport in paracellular channels. Although these share some properties with other widely studied transmembrane channels, they also bear relevant differences.

DOI: 10.1021/acs.jpcb.8b06484
J. Phys. Chem. B 2018, 122, 10783−10792

For example, ionotropic glutamate receptor channels have a pore diameter of 5.5−7.0 Å, similar to what we observe for the Cldn15 pore, and are able to permeate hydrated and partially hydrated cations across the membrane.[75] However, although in most channels ion permeation occurs through the fairly rigid regions of the proteins embedded in a membrane environment,[76,77] paracellular channels regulate transport parallel to the membrane planes, in the hydrated space between adjacent epithelial or endothelial cells. The Suzuki model, our refined version, and the only few others currently available,[24,25,31] all predict claudin channels with a pore region where the side chains of extracellular loops form the narrow filter and modulate selectivity. This arrangement results in a pore structure that is overall less rigid than in transmembrane channels and whose size is affected by the fluctuations of the extracellular loops, particularly ECL1.[29]

CONCLUSIONS

Claudin channels connect adjacent cells in TJs of biological barriers, regulating paracellular traffic in the aqueous, intercellular environment, and represent an exciting new class of selectively conducting molecular pores. Because of the lack of structural data, however, the atomic-level details of their mechanism are yet to be fully charted. Here, we employed the structural model of a Cldn15 channel that we have recently refined to investigate the transport properties of Na^+, K^+, and Cl^- ions via MD simulations in full atomic detail. The FE and kinetics calculations indicate that the model allows the flux of cations, whereas preventing that of chloride, consistently with what is expected for the Cldn15 channels. We quantify the charge selectivity property in terms of an FE well for cations and a barrier for anions and find a reduction of 1 order of magnitude in permeation timescales. Moreover, we observe that these properties correlate with the position of several acidic residues along the channel surface, in particular at the center of the pore. Our results provide an atom-detailed, quantitatively based picture of ionic transport in paracellular channels, demonstrating that our structural model captures the main physiological properties of these architectures in agreement with a broad experimental literature, and yield a validated molecular structure that will be crucial to study the detailed mechanism of paracellular transport in TJ channels of biological barriers.

ASSOCIATED CONTENT

Supporting Information

The Supporting Information is available free of charge on the ACS Publications website at DOI: 10.1021/acs.jpcb.8b06484.

Description of the Suzuki model for paracellular channels and details of the block analysis to estimate the errors in the US PMF (PDF)

AUTHOR INFORMATION

Corresponding Authors

*E-mail: fabio.benfenati@iit.it (F.B.).
*E-mail: luca.maragliano@iit.it (L.M.).

ORCID

Fabio Benfenati: 0000-0002-0653-8368
Luca Maragliano: 0000-0002-5705-6967

Notes

The authors declare no competing financial interest.

ACKNOWLEDGMENTS

Computing time allocations were granted by Cineca under the ISCRA initiative. This work has received funding from the European Union's Horizon 2020 Research and Innovation Programme under grant agreement no. 785219—Graphene-Core2. The authors are grateful to Grazia Cottone and Matteo Ceccarelli for useful discussions.

REFERENCES

(1) Furuse, M.; Fujita, K.; Hiiragi, T.; Fujimoto, K.; Tsukita, S. Claudin-1 and -2: Novel Integral Membrane Proteins Localizing at Tight Junctions with No Sequence Similarity to Occludin. *J. Cell Biol.* **1998**, *141*, 1539−1550.

(2) Morita, K.; Sasaki, H.; Furuse, M.; Tsukita, S. Endothelial Claudin. *J. Cell Biol.* **1999**, *147*, 185−194.

(3) Anderson, J. M. Molecular Structure of Tight Junctions and Their Role in Epithelial Transport. *News Physiol. Sci.* **2001**, *16*, 126−130.

(4) Farquhar, M. G.; Palade, G. E. Junctional Complexes in Various Epithelia. *J. Cell Biol.* **1963**, *17*, 375−412.

(5) Gumbiner, B. Structure, Biochemistry, and Assembly of Epithelial Tight Junctions. *Am. J. Physiol.: Cell Physiol.* **1987**, *253*, C749−C758.

(6) Krause, G.; Winkler, L.; Mueller, S. L.; Haseloff, R. F.; Piontek, J.; Blasig, I. E. Structure and Function of Claudins. *Biochim. Biophys. Acta* **2008**, *1778*, 631−645.

(7) Powell, D. W. Barrier Function of Epithelia. *Am. J. Physiol.: Gastrointest. Liver Physiol.* **1981**, *241*, G275−G288.

(8) Tang, V. W.; Goodenough, D. A. Paracellular Ion Channel at the Tight Junction. *Biophys. J.* **2003**, *84*, 1660−1673.

(9) Zihni, C.; Mills, C.; Matter, K.; Balda, M. S. Tight Junctions: From Simple Barriers to Multifunctional Molecular Gates. *Nat. Rev. Mol. Cell Biol.* **2016**, *17*, 564−580.

(10) Furuse, M.; Sasaki, H.; Fujimoto, K.; Tsukita, S. A Single Gene Product, Claudin-1 or -2, Reconstitutes Tight Junction Strands and Recruits Occludin in Fibroblasts. *J. Cell Biol.* **1998**, *143*, 391−401.

(11) Rosenthal, R.; Milatz, S.; Krug, S. M.; Oelrich, B.; Schulzke, J.-D.; Amasheh, S.; Günzel, D.; Fromm, M. Claudin-2, a Component of the Tight Junction, Forms a Paracellular Water Channel. *J. Cell Sci.* **2010**, *123*, 1913−1921.

(12) Günzel, D.; Yu, A. S. L. Claudins and the Modulation of Tight Junction Permeability. *Physiol. Rev.* **2013**, *93*, 525−569.

(13) Wen, H.; Watry, D. D.; Marcondes, M. C. G.; Fox, H. S. Selective Decrease in Paracellular Conductance of Tight Junctions: Role of the First Extracellular Domain of Claudin-5. *Mol. Cell. Biol.* **2004**, *24*, 8408−8417.

(14) Milatz, S.; Krug, S. M.; Rosenthal, R.; Günzel, D.; Müller, D.; Schulzke, J.-D.; Amasheh, S.; Fromm, M. Claudin-3 Acts as a Sealing Component of the Tight Junction for Ions of Either Charge and Uncharged Solutes. *Biochim. Biophys. Acta* **2010**, *1798*, 2048−2057.

(15) Amasheh, S.; Schmidt, T.; Mahn, M.; Florian, P.; Mankertz, J.; Tavalali, S.; Gitter, A. H.; Schulzke, J.-D.; Fromm, M. Contribution of Claudin-5 to Barrier Properties in Tight Junctions of Epithelial Cells. *Cell Tissue Res.* **2005**, *321*, 89−96.

(16) Veshnyakova, A.; Krug, S. M.; Mueller, S. L.; Piontek, J.; Protze, J.; Fromm, M.; Krause, G. Determinants Contributing to Claudin Ion Channel Formation. *Ann. N. Y. Acad. Sci.* **2012**, *1257*, 45−53.

(17) Hou, J.; Goodenough, D. A. Claudin-16 and Claudin-19 Function in the Thick Ascending Limb. *Curr. Opin. Nephrol. Hypertens.* **2010**, *19*, 483−488.

(18) Suzuki, H.; Nishizawa, T.; Tani, K.; Yamazaki, Y.; Tamura, A.; Ishitani, R.; Dohmae, N.; Tsukita, S.; Nureki, O.; Fujiyoshi, Y. Crystal Structure of a Claudin Provides Insight into the Architecture of Tight Junctions. *Science* **2014**, *344*, 304−307.

(19) Saitoh, Y.; Suzuki, H.; Tani, K.; Nishikawa, K.; Irie, K.; Ogura, Y.; Tamura, A.; Tsukita, S.; Fujiyoshi, Y. Structural Insight Into Tight Junction Disassembly by Clostridium Perfringens Enterotoxin. *Science* **2015**, *347*, 775−778.

DOI: 10.1021/acs.jpcb.8b06484
J. Phys. Chem. B 2018, 122, 10783−10792

(20) Shinoda, T.; Shinya, N.; Ito, K.; Ohsawa, N.; Terada, T.; Hirata, K.; Kawano, Y.; Yamamoto, M.; Kimura-Someya, T.; Yokoyama, S.; Shirouzu, M. Structural Basis for Disruption of Claudin Assembly in Tight Junctions by An Enterotoxin. *Sci. Rep.* **2016**, *6*, 33632.
(21) Colegio, O. R.; Van Itallie, C. M.; McCrea, H. J.; Rahner, C.; Anderson, J. M. Claudins Create Charge-Selective Channels in the Paracellular Pathway Between Epithelial Cells. *Am. J. Physiol.: Cell Physiol.* **2002**, *283*, C142−C147.
(22) Goliaei, A.; Adhikari, U.; Berkowitz, M. L. Opening of the Blood-Brain Barrier Tight Junction Due to Shock Wave Induced Bubble Collapse: A Molecular Dynamics Simulation Study. *ACS Chem. Neurosci.* **2015**, *6*, 1296−1301.
(23) Irudayanathan, F. J.; Trasatti, J. P.; Karande, P.; Nangia, S. Molecular Architecture of the Blood Brain Barrier Tight Junction Proteins-A Synergistic Computational and In Vitro Approach. *J. Phys. Chem. B* **2015**, *120*, 77−88.
(24) Irudayanathan, F. J.; Wang, N.; Wang, X.; Nangia, S. Architecture of the Paracellular Channels Formed by Claudins of the Blood-brain Barrier Tight Junctions. *Ann. N. Y. Acad. Sci.* **2017**, *1405*, 131−146.
(25) Irudayanathan, F. J.; Wang, X.; Wang, N.; Willsey, S. R.; Seddon, I. A.; Nangia, S. Self-Assembly Simulations of Classic Claudins-Insights into the Pore Structure, Selectivity, and Higher Order Complexes. *J. Phys. Chem. B* **2018**, *122*, 7463−7474.
(26) Suzuki, H.; Tani, K.; Tamura, A.; Tsukita, S.; Fujiyoshi, Y. Model for the Architecture of Claudin-Based Paracellular Ion Channels through Tight Junctions. *J. Mol. Biol.* **2015**, *427*, 291−297.
(27) Colegio, O. R.; Van Itallie, C.; Rahner, C.; Anderson, J. M. Claudin Extracellular Domains Determine Paracellular Charge Selectivity And Resistance but Not Tight Junction Fibril Architecture. *Am. J. Physiol.: Cell Physiol.* **2003**, *284*, C1346−C1354.
(28) Krause, G.; Protze, J.; Piontek, J. Assembly and Function of Claudins: Structure-Function Relationships Based on Homology Models and Crystal Structures. *Semin. Cell Dev. Biol.* **2015**, *42*, 3−12.
(29) Alberini, G.; Benfenati, F.; Maragliano, L. A Refined Model of Claudin-15 Tight Junction Paracellular Architecture by Molecular Dynamics Simulations. *PLoS One* **2017**, *12*, No. e0184190.
(30) Zhao, J.; Krystofiak, E. S.; Ballesteros, A.; Cui, R.; Van Itallie, C. M.; Anderson, J. M.; Fenollar-Ferrer, C.; Kachar, B. Multiple Claudin-Claudin Cis Interfaces Are Required for Tight Junction Strand Formation and Inherent Flexibility. *Communications Biology* **2018**, *1*, 50.
(31) Samanta, P.; Wang, Y.; Fuladi, S.; Zou, J.; Li, Y.; Shen, L.; Weber, C.; Khalili-Araghi, F. Molecular Determination of Claudin-15 Organisation And Channel Selectivity. *J. Gen. Physiol.* **2018**, *150*, 949−968.
(32) Torrie, G. M.; Valleau, J. P. Nonphysical Sampling Distributions in Monte Carlo Free-energy Estimation: Umbrella Sampling. *J. Comput. Phys.* **1977**, *23*, 187−199.
(33) Faradjian, A. K.; Elber, R. Computing Time Scales from Reaction Coordinates By Milestoning. *J. Chem. Phys.* **2004**, *120*, 10880−10889.
(34) Maragliano, L.; Vanden-Eijnden, E.; Roux, B. Free Energy and Kinetics of Conformational Transitions from Voronoi Tessellated Milestoning with Restraining Potentials. *J. Chem. Theory Comput.* **2009**, *5*, 2589−2594.
(35) Kumar, S.; Rosenberg, J. M.; Bouzida, D.; Swendsen, R. H.; Kollman, P. A. The Weighted Histogram Analysis Method for Free-energy Calculations On Biomolecules. I. The method. *J. Comput. Chem.* **1992**, *13*, 1011−1021.
(36) Souaille, M.; Roux, B. Extension to the Weighted Histogram Analysis Method: Combining Umbrella Sampling with Free Energy Calculations. *Comput. Phys. Commun.* **2001**, *135*, 40−57.
(37) Dellago, C.; Bolhuis, P. G.; Chandler, D. On the Calculation of Reaction Rate Constants in the Transition Path Ensemble. *J. Chem. Phys.* **1999**, *110*, 6617−6625.
(38) Allen, R. J.; Valeriani, C.; ten Wolde, P. R. Forward Flux Sampling for Rare Event Simulations. *J. Phys.: Condens. Matter* **2009**, *21*, 463102.
(39) Tiwary, P.; Parrinello, M. From Metadynamics to Dynamics. *Phys. Rev. Lett.* **2013**, *111*, 230602.
(40) Vanden-Eijnden, E.; Venturoli, M. Markovian Milestoning with Voronoi Tessellations. *J. Chem. Phys.* **2009**, *130*, 194101.
(41) Yu, T.-Q.; Lapelosa, M.; Vanden-Eijnden, E.; Abrams, C. F. Full Kinetics of CO Entry, Internal Diffusion, and Exit in Myoglobin from Transition-Path Theory Simulations. *J. Am. Chem. Soc.* **2015**, *137*, 3041−3050.
(42) E, W.; Vanden-Eijnden, E. Transition-Path Theory and Path-finding Algorithms For the Study of Rare Events. *Annu. Rev. Phys. Chem.* **2010**, *61*, 391−420.
(43) Feller, S. E.; Zhang, Y.; Pastor, R. W.; Brooks, B. R. Constant Pressure Molecular Dynamics Simulation: The Langevin Piston Method. *J. Chem. Phys.* **1995**, *103*, 4613−4621.
(44) Martyna, G. J.; Tobias, D. J.; Klein, M. L. Constant Pressure Molecular Dynamics Algorithms. *J. Chem. Phys.* **1994**, *101*, 4177−4189.
(45) Phillips, J. C.; Braun, R.; Wang, W.; Gumbart, J.; Tajkhorshid, E.; Villa, E.; Chipot, C.; Skeel, R. D.; Kalé, L.; Schulten, K. Scalable Molecular Dynamics with NAMD. *J. Comput. Chem.* **2005**, *26*, 1781−1802.
(46) Best, R. B.; Zhu, X.; Shim, J.; Lopes, P. E. M.; Mittal, J.; Feig, M.; MacKerell, A. D. Optimization of the Additive CHARMM All-Atom Protein Force Field Targeting Improved Sampling of the Backbone ϕ, ψ and Side-Chain χ1 and χ2 Dihedral Angles. *J. Chem. Theory Comput.* **2012**, *8*, 3257−3273.
(47) Klauda, J. B.; Venable, R. M.; Freites, J. A.; O'Connor, J. W.; Tobias, D. J.; Mondragon-Ramirez, C.; Vorobyov, I.; MacKerell, A. D.; Pastor, R. W. Update of the CHARMM All-Atom Additive Force Field for Lipids: Validation on Six Lipid Types. *J. Phys. Chem. B* **2010**, *114*, 7830−7843.
(48) Jorgensen, W. L.; Chandrasekhar, J.; Madura, J. D.; Impey, R. W.; Klein, M. L. Comparison of Simple Potential Functions for Simulating Liquid Water. *J. Chem. Phys.* **1983**, *79*, 926−935.
(49) Darden, T.; York, D.; Pedersen, L. Particle mesh Ewald: An N·log(N) method for Ewald sums in large systems. *J. Chem. Phys.* **1993**, *98*, 10089−10092.
(50) Ryckaert, J.-P.; Ciccotti, G.; Berendsen, H. J. C. Numerical Integration of The Cartesian Equations of Motion of a System with Constraints: Molecular Dynamics of N-alkanes. *J. Comput. Phys.* **1977**, *23*, 327−341.
(51) Fiorin, G.; Klein, M. L.; Hénin, J. Using Collective Variables to Drive Molecular Dynamics Simulations. *Mol. Phys.* **2013**, *111*, 3345−3362.
(52) Pettersen, E. F.; Goddard, T. D.; Huang, C. C.; Couch, G. S.; Greenblatt, D. M.; Meng, E. C.; Ferrin, T. E. UCSF Chimera-A Visualization System for Exploratory Research and Analysis. *J. Comput. Chem.* **2004**, *25*, 1605−1612.
(53) Humphrey, W.; Dalke, A.; Schulten, K. VMD: Visual molecular dynamics. *J. Mol. Graphics* **1996**, *14*, 33−38.
(54) Smart, O. S.; Neduvelil, J. G.; Wang, X.; Wallace, B. A.; Sansom, M. S. P. HOLE: A Program for the Analysis of the Pore Dimensions of Ion Channel Structural Models. *J. Mol. Graphics* **1996**, *14*, 354−360.
(55) Smart, O. S.; Breed, J.; Smith, G. R.; Sansom, M. S. A Novel Method for Structure-based Prediction of Ion Channel Conductance Properties. *Biophys. J.* **1997**, *72*, 1109−1126.
(56) Yu, A. S. L.; Cheng, M. H.; Angelow, S.; Günzel, D.; Kanzawa, S. A.; Schneeberger, E. E.; Fromm, M.; Coalson, R. D. Molecular Basis for Cation Selectivity in Claudin-2-based Paracellular Pores: Identification of an Electrostatic Interaction Site. *J. Gen. Physiol.* **2008**, *133*, 111−127.
(57) Krug, S. M.; Günzel, D.; Conrad, M. P.; Lee, I.-F. M.; Amasheh, S.; Fromm, M.; Yu, A. S. L. Charge-selective claudin channels. *Ann. N. Y. Acad. Sci.* **2012**, *1257*, 20−28.

DOI: 10.1021/acs.jpcb.8b06484
J. Phys. Chem. B 2018, 122, 10783−10792

(58) Allen, T. W.; Kuyucak, S.; Chung, S.-H. Molecular Dynamics Study of the KcsA Potassium Channel. *Biophys. J.* **1999**, *77*, 2502–2516.
(59) Khalili-Araghi, F.; Tajkhorshid, E.; Schulten, K. Dynamics of K + ion conduction through Kv1.2. *Biophys J* **2006**, *91*, L72–L74.
(60) Noskov, S. Y.; Roux, B. Importance of Hydration and Dynamics on the Selectivity of the KcsA and NaK Channels. *J. Gen. Physiol.* **2007**, *129*, 135–143.
(61) Bostick, D. L.; Brooks, C. L. Selectivity in K+ channels is due to topological control of the permeant ion's coordinated state. *Proc. Natl. Acad. Sci. U.S.A.* **2007**, *104*, 9260–9265.
(62) Corry, B.; Thomas, M. Mechanism of Ion Permeation and Selectivity in a Voltage Gated Sodium Channel. *J. Am. Chem. Soc.* **2012**, *134*, 1840–1846.
(63) Ulmschneider, M. B.; Bagnéris, C.; McCusker, E. C.; DeCaen, P. G.; Delling, M.; Clapham, D. E.; Ulmschneider, J. P.; Wallace, B. A. Molecular Dynamics of Ion Transport Through the Open Conformation of a Bacterial Voltage-gated Sodium Channel. *Proc. Natl. Acad. Sci. U.S.A.* **2013**, *110*, 6364–6369.
(64) Boiteux, C.; Vorobyov, I.; Allen, T. W. Ion Conduction and Conformational Flexibility of a Bacterial Voltage-gated Sodium Channel. *Proc. Natl. Acad. Sci. U.S.A.* **2014**, *111*, 3454–3459.
(65) Domene, C.; Barbini, P.; Furini, S. Bias-Exchange Metadynamics Simulations: An Efficient Strategy for the Analysis of Conduction and Selectivity in Ion Channels. *J. Chem. Theory Comput.* **2015**, *11*, 1896–1906.
(66) Guardiani, C.; Rodger, P. M.; Fedorenko, O. A.; Roberts, S. K.; Khovanov, I. A. Sodium Binding Sites and Permeation Mechanism in the NaChBac Channel: A Molecular Dynamics Study. *J. Chem. Theory Comput.* **2017**, *13*, 1389–1400.
(67) Van Itallie, C. M.; Fanning, A. S.; Anderson, J. M. Reversal of Charge Selectivity in Cation or Anion-selective Epithelial Lines by Expression of Different Claudins. *Am. J. Physiol.: Renal, Fluid Electrolyte Physiol.* **2003**, *285*, F1078–F1084.
(68) Kottra, G.; Frömter, E. Functional properties of the paracellular pathway in some leaky epithelia. *J Exp Biol* **1983**, *106*, 217–229.
(69) Weber, C. R.; Liang, G. H.; Wang, Y.; Das, S.; Shen, L.; Yu, A. S. L.; Nelson, D. J.; Turner, J. R. Claudin-2-dependent Paracellular Channels Are Dynamically Gated. *eLife* **2015**, *4*, No. e09906.
(70) Zhu, F.; Hummer, G. Theory and Simulation of Ion Conduction in the Pentameric GLIC Channel. *J. Chem. Theory Comput.* **2012**, *8*, 3759–3768.
(71) Bernèche, S.; Roux, B. Energetics of Ion Conduction Through the K+ Channel. *Nature* **2001**, *414*, 73–77.
(72) Jensen, M. Ø.; Borhani, D. W.; Lindorff-Larsen, K.; Maragakis, P.; Jogini, V.; Eastwood, M. P.; Dror, R. O.; Shaw, D. E. Principles Of Conduction and Hydrophobic Gating in K+ Channels. *Proc. Natl. Acad. Sci. U.S.A.* **2010**, *107*, 5833–5838.
(73) Allen, T. W.; Andersen, O. S.; Roux, B. Molecular Dynamics - Potential of Mean Force Calculations as a Tool for Understanding Ion Permeation and Selectivity in Narrow Channels. *Biophys. Chem.* **2006**, *124*, 251–267.
(74) Allen, T. W.; Andersen, O. S.; Roux, B. Energetics of Ion Conduction Through The Gramicidin Channel. *Proc. Natl. Acad. Sci. U.S.A.* **2004**, *101*, 117–122.
(75) Villarroel, A.; Burnashev, N.; Sakmann, B. Dimensions of the Narrow Portion of a Recombinant Nmda Receptor Channel. *Biophys. J.* **1995**, *68*, 866–875.
(76) Taly, A.; Hénin, J.; Changeux, J.-P.; Cecchini, M. Allosteric regulation of pentameric ligand-gated ion channels: An emerging mechanistic perspective. *Channels* **2014**, *8*, 350–360.
(77) Roux, B. Ion Channels and Ion Selectivity. *Essays Biochem.* **2017**, *61*, 201–209.

DOI: 10.1021/acs.jpcb.8b06484
J. Phys. Chem. B 2018, 122, 10783–10792